ANL-21/35

Performance Validation of Pulsed Thermal Imaging System for In-Service Applications

Pulsed Thermal Tomography Nondestructive Examination of Additively Manufactured Reactor Materials and Components

Nuclear Science and Engineering Division

ANL-21/35

Performance Validation of Pulsed Thermal Imaging System for In-Service Applications

Pulsed Thermal Tomography Nondestructive Examination of Additively Manufactured Reactor Materials and Components

prepared by
Alexander Heifetz[1], Xin Zhang[1,2], Jafar Saniie[2], Sasan Bakhtiari[1]

[1]Nuclear Science Engineering Division, Argonne National Laboratory
[2]Department of Electrical and Computer Engineering, Illinois Institute of Technology, Chicago, IL

August 16, 2021

Table of Contents

List of Figures

Abstract

Additive manufacturing (AM) is an emerging method for cost-efficient fabrication of complex topology nuclear reactor parts from high-strength corrosion resistance alloys, such as stainless steel and Inconel. AM of metallic structures for nuclear energy applications is currently based on laser powder bed fusion (LPBF) process, which has the capability of melting metallic powder and net shaping the structures with relatively high precision. Some of the challenges with using LPBF method for nuclear manufacturing include the possibility of introducing pores into metallic structures. Integrity of AM structures needs to be evaluated nondestructively because material flaws could lead to premature failures in high temperature nuclear reactor environment. Currently, there exist limited capabilities to evaluate actual AM structures non-destructively. Pulsed Thermography Imaging (PTI) provides a capability for non-destructive evaluation (NDE) of sub-surface defects in arbitrary size structures. The PTI method is based on recording material surface temperature transients with infrared (IR) camera following thermal pulse delivered on material surface with flash light. The PTI method has advantages for NDE of actual AM structures because the method involves one-sided non-contact measurements and fast processing of large sample areas captured in one image. Following initial qualification of an AM component for deployment in a nuclear reactor, a PTI system can also be used for in-service nondestructive evaluation (NDE) applications. In this report, we describe recent progress in enhancing PTI capabilities in detecting microscopic defects in metallic specimens. SS316 and IN718 specimens were developed with a pattern of subsurface calibrated flat bottom hole (FBH) defects with diameters from 500µm to 200µm. FBH's were created with EDM (electron discharge machininig) drill. PTI imaging data was processed Spatial Temporal Denoised Thermal Source Separation (STDTSS) unsupervised machine learning (ML) algorithm. We show that defects as small as 200µm in SS316 and IN718 can be detected with STDTSS algorithm. To the best of our knowledge, these are the smallest detected defects which are reported in literature.

1. Introduction

Additive manufacturing (AM) of metals is an emerging method for cost-efficient production of low volume custom structures for industries, such as nuclear energy [1]. Metals of interest for nuclear applications typically include high-strength corrosion-resistant alloys, such as stainless steel 316L (SS316L) and Inconel 718 (IN718). Because of high melting temperature, AM of SS316L and IN718 is currently based on laser powder-bed fusion (LPBF) process [2]. Due to the intrinsic features of LPBF process, pores can appear in 3D printed metallic structures [2]. With the exposure to high temperature and creep damage in high-temperature nuclear reactors, a pore can potentially become a seed for cracking [3]. Because of stringent safety requirements, each AM metallic structure needs to be qualified through nondestructive examination before deployment in a nuclear reactor [4]. If a defect is discovered, either a flaw mitigation with heat treatment can be performed, or the part could be disqualified from service.

Typical porosity defects observed in LPBF manufacturing consist of spheroidal-shape keyhole pores caused by excessive laser power, irregular-shape lack of fusion (LOF) pores caused by insufficient laser power, and spherical gas pores caused by trapped of gas in solidifying melt pool. Sizes of pores depend on the quality of the LPBF process. Typical sizes of keyhole and LOF pores in tens to hundreds of microns, while gas pores sizes are on the order of a few microns [5]. Prior studies indicate that larger size pores located closer to surface are more likely to cause fatigue crack initiation. High-resolution imaging with X-ray or neutron computed tomography (CT) can be used for imaging pores in small coupons to evaluate quality of LPBF process. However, applications of X-ray or neutron CT to NDE of actual AM structures are limited because of large size, lack of symmetry and complex shapes of AM structures. Ultrasonic testing is scalable with structure size, but face challenges because the rough surfaces, characteristic of AM structures, affect the probe coupling. For high-resolution ultrasonic tomography, imaging of large structures is time-consuming because of point-by-point raster scanning of specimens [6].

We investigate Infrared Pulsed Thermal Imaging (PTI) for detection of subsurface microscopic pores in AM structures. This method offers several potential advantages because PTI measurements are one-sided, non-contact, and scalable to arbitrary size structures [7]. The PTI method consists of recording material surface temperature transients with an infrared (IR) camera, following deposition of thermal impulse on material surface with a flash lamp. Material defects can be detected by analyzing thermograms (data cube of sequentially recorded surface temperatures).

In prior studies, we have demonstrated the capability of PTI in detection of calibrated defects in SS316L and IN718. The calibrated defects consisted of (1) hemispherical regions containing un-sintered powder, which were imprinted into metallic specimens during LPBF manufacturing, (2) flat bottom hole (FBH) indentations in metallic specimens. In prior work, the smallest detected defect, either an imprinted hemisphere or an FBH was a 1mm-diameter feature. The objective of the study in this report is to achieve detection of microscopic defects. For such defects, thermal signature intensity is approaching the detection sensitivity level of IR camera. Extraction of features of interest from PTI images can be accomplished with machine learning (ML) and image

processing algorithms. In a recent work, we have developed Spatial Temporal Denoised Thermal Source Separation (STDTSS) ML algorithm for processing PTI images [14]. The STDTSS involves spatial and temporal denoising using Gaussian filtering [15] and Savitzky–Golay filtering [16], followed by the matrix decomposition using Principal Component Analysis (PCA) [15], and Independent Component Analysis (ICA) [17], to automatically detect flaws in images.

In the work described in this report, we use STDTSS algorithm for processing of PTI images of metallic specimens with microscopic FBH defects created with EDM (electron discharge machining drill). The subsurface defects ranged from 200µm to 500µm in diameter, with depths below the surface ranging from 100µm to 500µm. We show that all FBH defects are detectable in SS316 and IN718 specimens at depths smaller than 400µm.

2. Infrared Pulsed Thermal Imaging System

2.1. Experimental System Setup

In the experimental PTI system, data is acquired with a laboratory setup consisting of a megapixel fast frame infrared (IR) camera and flash lamp is shown in Figure 1. A schematic depiction of the setup is shown in Figure 1(a), while the photograph of the laboratory system is presented in Figure 1(b). A pulse trigger sends a signal to capacitor to discharge in a circuit containing white light flash lamp. The flash lamp source Balcar ASYM 6400 delivers a pulse of 6400J/2ms thermal energy to material surface. The flash lamp is typically positioned at 30cm to 50cm distance to the specimen under investigation. The exact distance and angle of illumination of the flash lamp are determined experimentally for each specimen. This is decided by positioning the IR camera at the focal length of the lens, and placing the flash lamp such that the IR field of view is not blocked, nor does IR camera block the flash.

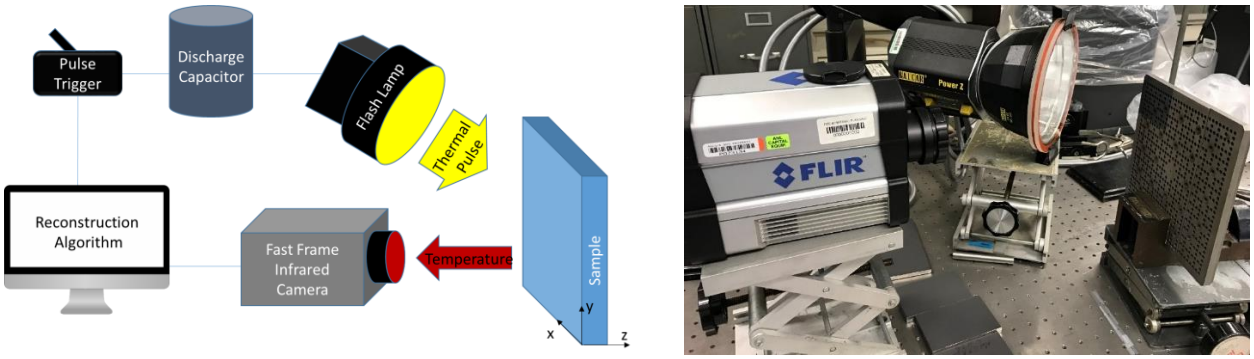

(a) (b)

Figure 1 – Flash thermography experimental setup: (a) Schematic drawing (b) Photograph of actual laboratory PTI system.

Heat transfer takes place from the heated surface to the interior of the sample, resulting in a continuous decrease of the surface temperature. Temporal profile at one location on the plate recorded with a calibrated IR camera is shown in Figure 2. For this particular location on the plate, temperature rises by approximately 50^{o}C. For better heat absorption, and to remove the effect of different surface emissivity, all materials in this study were spray-painted with washable graphite paint. Distribution of temperature on the plate surface can be non-uniform across the plate because flash lamp light is incident at an angle, and because drying paint can aggregate into localized clumps with spatially varying heat absorption characteristics.

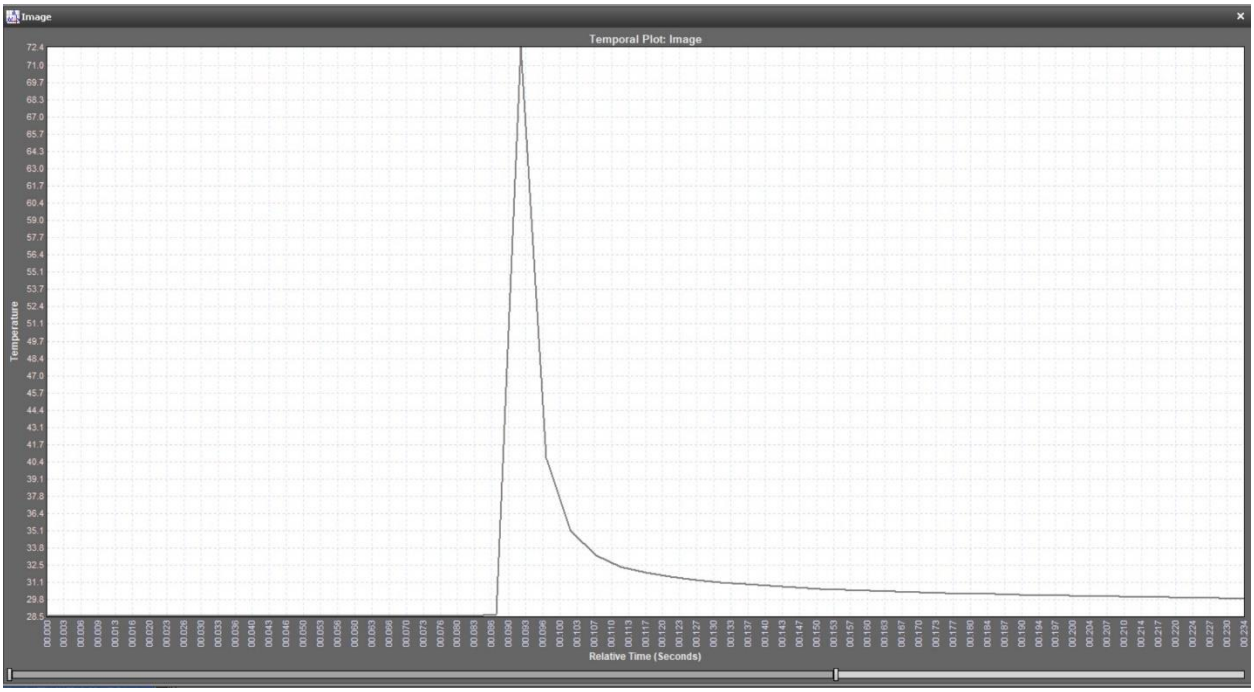

Figure 2 – Temperature transients on plate surface measured with calibrated IR camera at one pixel location

A megapixel fast frame infrared (IR) camera records blackbody radiation to obtain time-resolved images of surface temperature distribution T(x,y,t). The acquired thermal-imaging data cube therefore consist of a series of 2D images of the sample's surface temperature at consecutive time instants. The laboratory system shown in Figure 1 uses a FLIR x8501sc with Indium Antimonide (InSb) detector camera, which has integration time of 270ns, NETD sensitivity of <30mK, and frame rate of at least 180Hz. As heat deposited with flash lamp the surface starts diffusing into the material bulk, presence of low-density internal material inclusions is revealed through appearance of local temperature "hot spots" on the surface. This effect occurs because low density defects have lower thermal diffusivity compared with solid material. The defects act as thermal resistances and slow down thermal diffusion, which causes temperature difference on the material surface between regions of defects and non-defects. The feature of temperature difference on material surface is used for internal defects detection. However, the intensity of the feature can distorted due to thermal imaging noises, and uneven heating of specimens.

2.2. Spatial Temporal Denoised Thermal Source Separation (STDTSS) Machine Learning Algorithm

In thermography images of microscopic defects, signals from features are approaching the NETD limit. Therefore, image processing is required to separate signals due to defects from noises due to uneven heating and camera noises. We have recently developed image processing STDTSS algorithm which compensates for PT image artifacts to enable detection of flaws [14]. The flow chart of STDTSS algorithm is shown in Figure 3. The STDTSS algorithm incorporates a number

of image denoising features into the STDTSS algorithm. In particular, we design a Gaussian spatial filter and a 7-point Savitzky–Golay temporal filter as preprocessing steps to remove IR imaging noises in space and time. Next, PCA is used to decompose thermography data into principal features, which are fed into ICA implemented as a two-layer neural network structure. The ICA aims to classify and separate the thermography source signals, which correspond to image regions of defects, non-defects, and noise. Each thermography source signal exhibits different temperature evolution during the transient response recorded with PT system. We reconstruct the Thermal Source Image (TSI) from STDTSS to display image regions of defects to detect flaws.

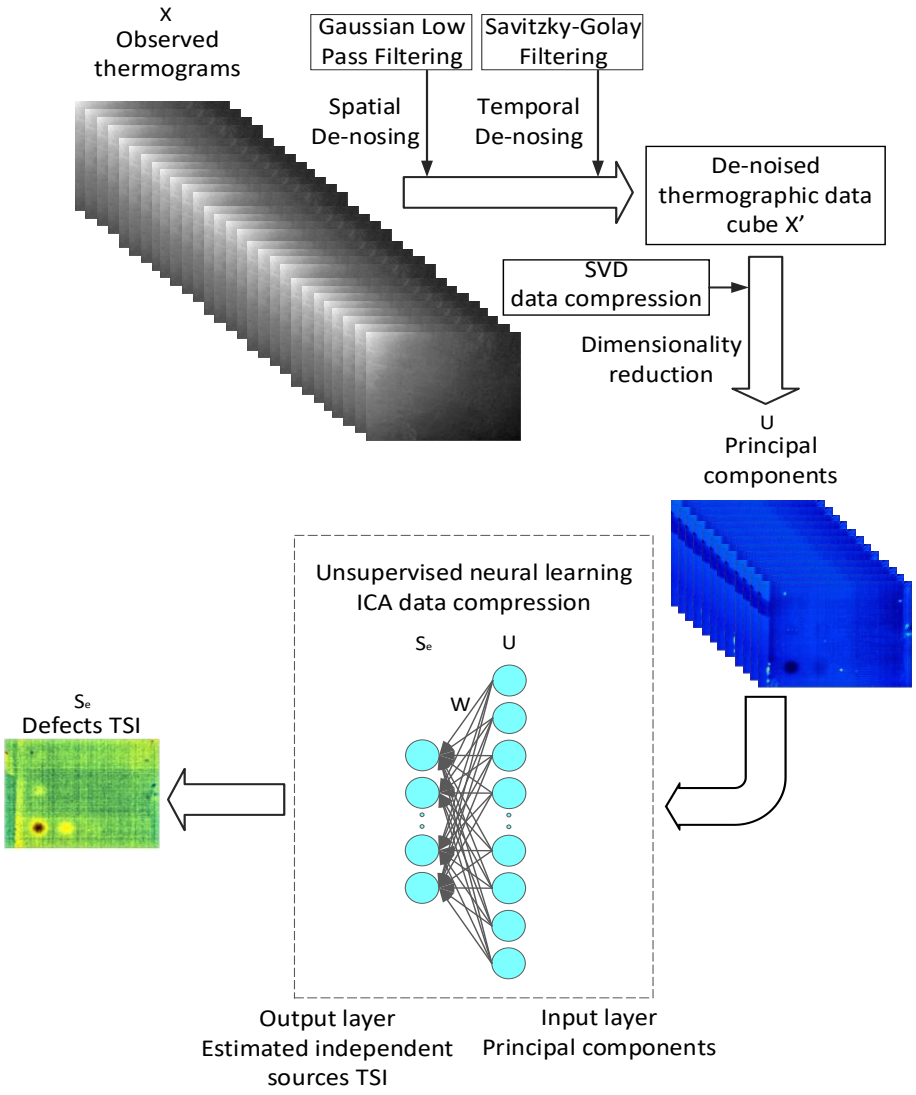

Figure 3 – Flowchart of STDTSS algorithm

3. Development of Microscopic Flat Bottom Hole Defects in SS316 and IN718 Plates

Calibrated FBH defects were introduced into SS316 and IN718 specimens with EDM drill. Prior studies of PTI performance involved calibrated defects introduced as either FBH defects created in metallic specimens with a high-strength drill, or hemispherical inclusions containing un-sintered trapped powder imprinted into metallic specimens during LPBF process. Creating microscopic calibrated defects in high strength metal is a challenge with LPBF process involves sintering SS316 and IN718 metallic powder grains with the average diameters of 20μm and 40μm, respectively. A scanning electron microscope (SEM) micrograph of SS316 TrueForm powder grains is shown in Figure 4(a). The histogram of particle diameter distribution is plotted in Figure 4(b). From the plot, one can observe that particle diameters can be as large as 50μm. Creating imprinted porosity defects with diameters smaller than 300μm with LPBF involves trapping several un-sintered powder grains. Controlling inclusion size at this length-scale is a difficult task because heat diffusion is involved in sintering. In addition, LOF and keyhole inclusion are typically air voids in metal with no trapped powder.

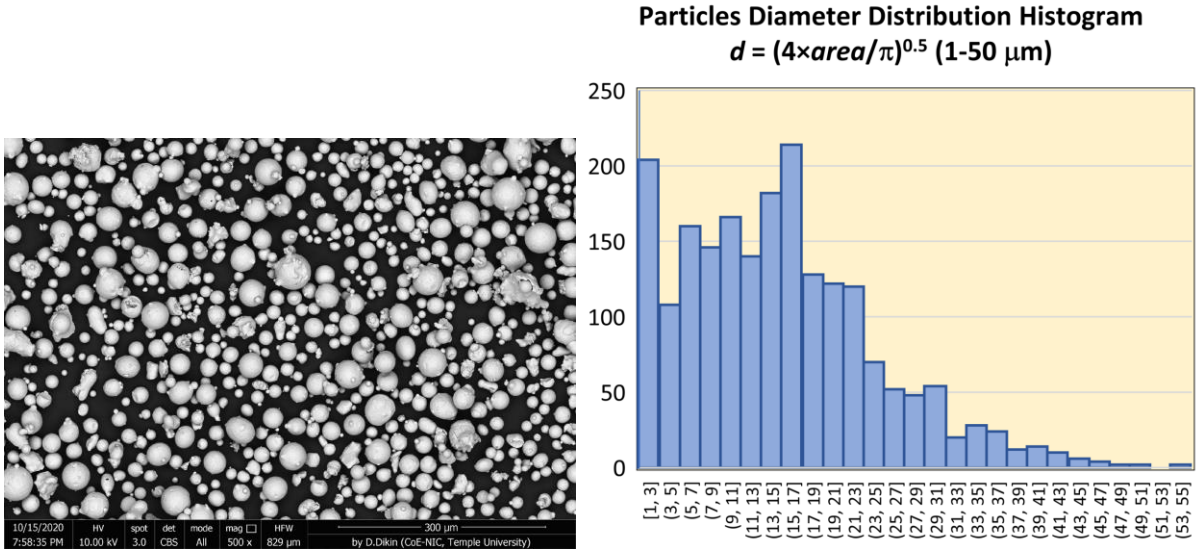

(a) (b)

Figure 4 – (a) Photograph of EDM-drilled microscopic FBH's in SS316 plate. (b) Back surface of the plate painted with Krylon ultra flat black spray paint.

Therefore, in developing microscopic calibrated defects, the FBH model of material defect for proof-of-principle studies was selected. FBH defects closely model air voids from heat transfer physics point of view. FBH's can be created to be of precise shapes, diameters and depths relative material surface with an EDM drill. A pattern of microscopic FBH defects introduced into SS316 and IN718 plates with EDM drill is shown in Figure 5(a). There is a matrix of FBH's with diameters ϕ =500μm, 400μm, 300μm, and 200μm. The defects are located at depths d = 100μm, 200μm, 300μm, 400μm, and 500μm below the flat surface. The SS316 and IN718 plates are 3mm

thick. A photograph of the FBH's in SS316 plate is shown in Figure 5(b). A photograph of the flat side of the plate painted with Krylon ultra flat black spray paint is shown in Figure 5(c). Note that a 200µm FBH created with EDM drill in SS316 and IN718 3-mm thick plates corresponds the state-of-the-art limit for most EDM industry.

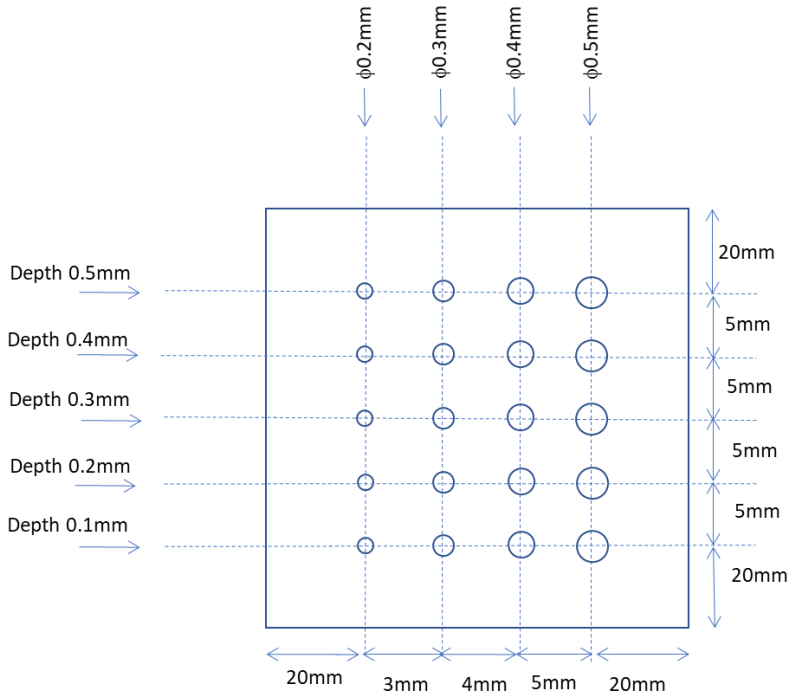

(a)

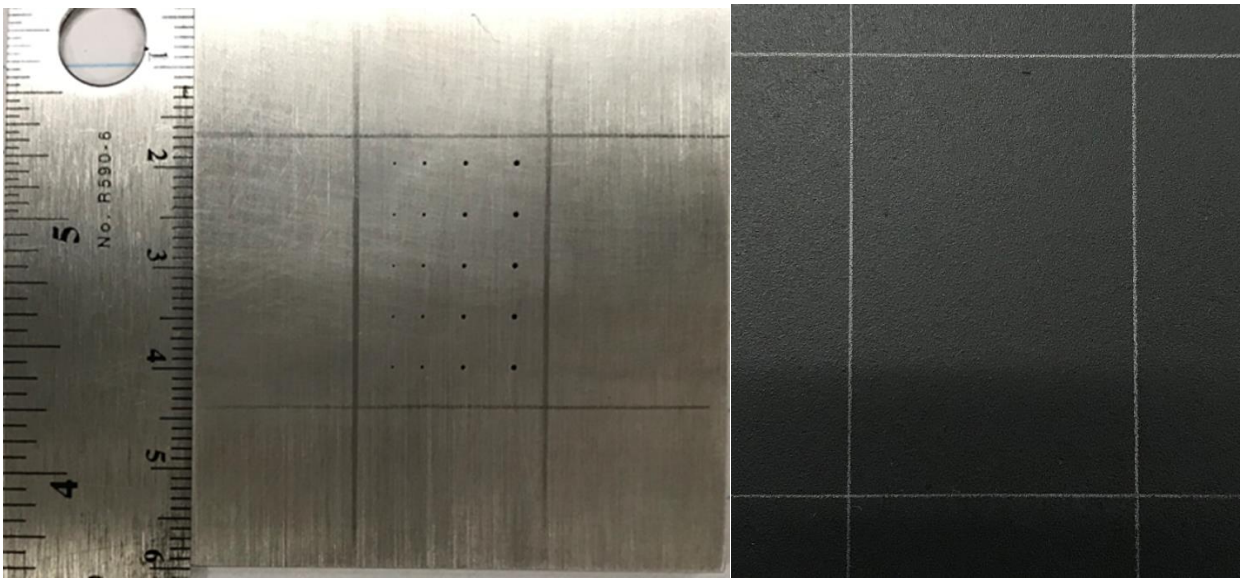

(b) (c)

Figure 5 – (a) Photograph of EDM-drilled microscopic FBH's in SS316 plate. (b) Back surface of the plate painted with Krylon ultra flat black spray paint.

4. Detection of Microscopic FBH Defects in SS316 and IN718 Plates with STDTSS Algorithm

In the first experiment, PTI imaging was performed on the SS316 plate. The measurements were made with the painted side plate (See Figure 4(c)) facing the IR camera and the flash lamp. Raw thermograms obtained from the IR camera, such as the one in Figure 6(a), do not show any defects. Image of the plate obtained with STDTSS algorithm is shown in Figure 6(b). All defects at depth at depths up to 300µm, and two larger defects at depth 400µm are clearly visible. To the best of our knowledge, detection of 200µm defect in SS316 is the smallest one reported in literature.

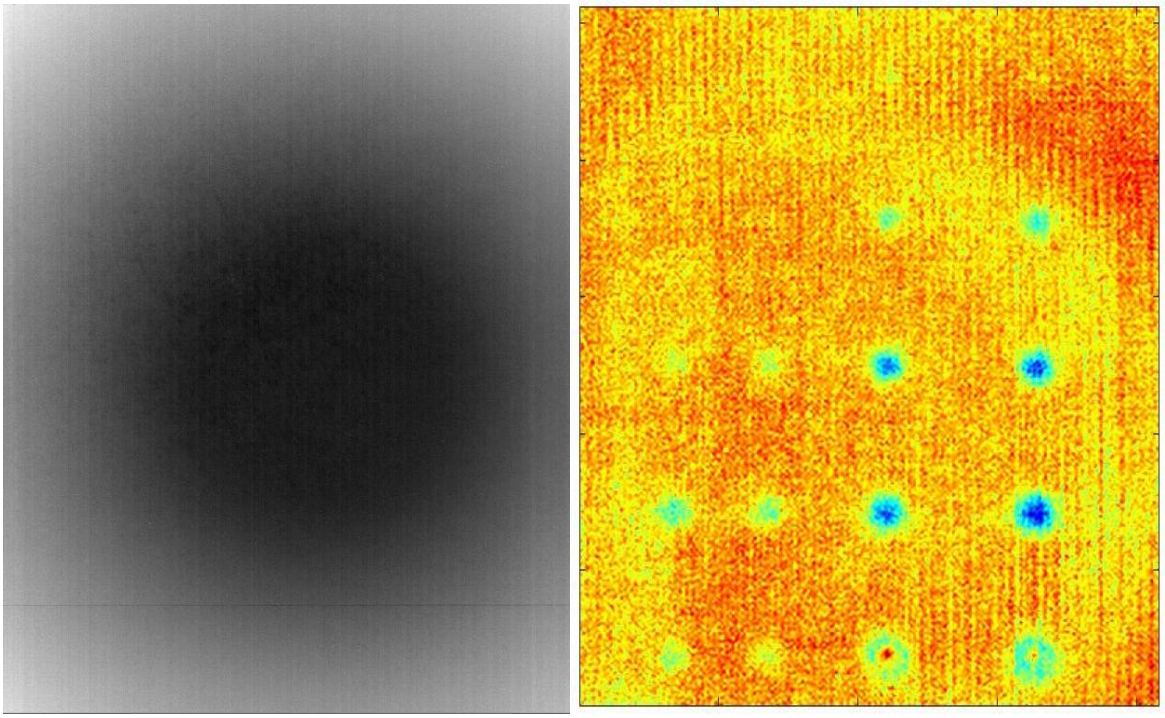

(a) (b)

Figure 6 – Results of STDTSS detection of microscopic FBH defects in SS316 specimen. (a) Raw thermogram. (b) STDTSS image.

In the second experiment, we repeated PTI measurements with the IN718 plate. Similar to the case described above, smaller pattern of defects imprinted into the AM SS316L plate. A raw termogram is shown in Figure 7(a). Image of defects obtained with STDTSS algorithm is shown in Figure 7(b). To the best of our knowledge, detection of 200µm in IN718 with PTI is the smallest reported defect detection in literature.

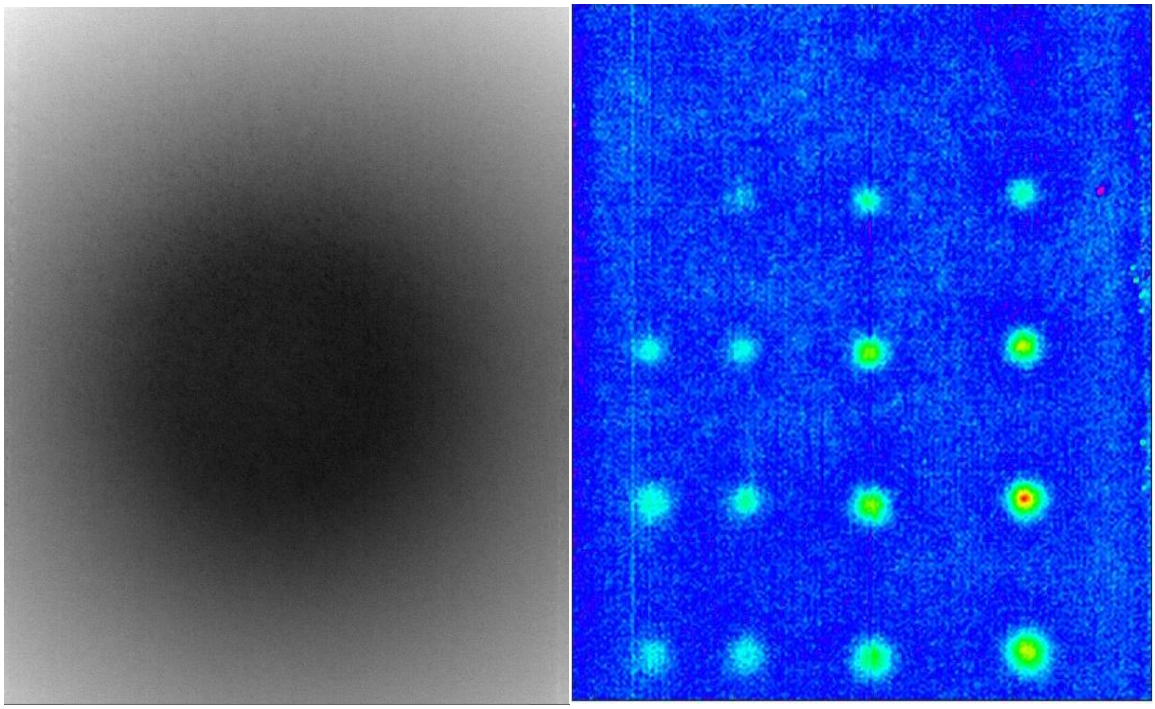

(a) (b)

Figure 7 – Results of STDTSS detection of microscopic defects in IN718 specimen. (a) Raw thermogram. (b) STDTSS image.

5. Conclusions

The PTI method has advantages for NDE of actual AM structures because the method involves one-sided non-contact measurements and fast processing of large sample areas captured in one image. Following initial qualification of an AM component for deployment in a nuclear reactor, a PTI system can also be used for in-service nondestructive evaluation (NDE) applications. In this report, we have investigated detection of microscopic subsurface defects in SS316 and IN718 specimens with PTI and ML-based STDTSS image processing algorithm. FBH defects with variable diameters and depths below the plate surface were created with EDM drilling. After PTI imaging, data was processed with STDTSS algorithm to obtain visualizations of the microscopic defects. To the best of our knowledge, detection of 200μm FBH with PTI is the smallest reported defect detection in NDE literature.

In future work, we will investigate detection of defects smaller than 200μm in SS316 and IN718. This is non-trivial because creating such defects requires special purpose microscopy EDM equipment, which is not widely available. To further enhance flaws detection, future work will involve optimizing the STDTSS by utilizing either sparse PCA or non-linear PCA. Further improvements in thermography hardware and ML algorithms would be needed to detect smaller and deeper-located defects, such as increasing the power of the flash lamp, and using a microscopic lens to increase the number of pixels per an image of a defect could enhance detection resolution.

References

1. X. Lou and D. Gandy, "Advanced Manufacturing for Nuclear Energy," JOM 71, 2834-2836 (2019).
2. S. A. Khairallah, A. T. Anderson, A. Rubenchik, W. E. King, "Laser Powder-Bed Fusion Additive Manufacturing: Physics of Complex Melt Flow and Formation Mechanisms of Pores, Spatter and Denudation Zones," Acta Materialia 108, 36-45 (2016).
3. M. D. Sangid, P. Ravi, V. Prithivirajan, N. A. Miller, P. Kenesei, J.-S. Park, "ICME Approach to Determining Critical Pore Size of IN718 Produced by Selective Laser Melting," JOM 72, 465-474 (2019).
4. X. Zhang, J. Saniie, W. Cleary, A. Heifetz. (2020). "Quality Control of Additively Manufactured Metallic Structures with Machine Learning of Thermography Images," JOM 72(12), 4682-4694 (2020).
5. X. Zhang, J. Saniie, A. Heifetz, "Detection of Defects in Additively Manufactured Stainless Steel 316L with Compact Infrared Camera and Machine Learning Algorithms," JOM 72(12), 4244-4253 (2020).
6. X. Zhang, B. Wang, J. Saniie, "Deep Convolutional Neural Networks Applied to Ultrasonic Images for Material Texture Recognition," 2020 IEEE International Ultrasonics Symposium (2020).
7. A. Heifetz, X. Zhang, J. Saniie, D. Shribak, T. Elmer, S. Bakhtiari, B. Khaykovich, W. L Cleary, "Second Annual Progress Report on Pulsed Thermal Tomography Nondestructive Examination of Additively Manufactured Reactor Materials," Argonne National Laboratory ANL-20/62 (2020).
8. X. Zhang, J. Saniie, A. Heifetz, "Neural Learning Based Blind Source Separation for Detection of Material Defects in Pulsed Thermography Images," 2020 IEEE International Conference on Electro-Information Technology (EIT), 112-116 (2020).
9. A. Heifetz, D. Shribak, X. Zhang, J. Saniie, Z.L. Fisher, T. Liu, J.G. Sun, T. Elmer, S. Bakhtiari, W. Cleary, "Thermal Tomography 3D Imaging of Additively Manufactured Metallic Structures," AIP Advances 10(10), 105318 (2020).
10. A. Heifetz, J.G. Sun, D. Shribak, T. Liu, T.W. Elmer, P. Kozak, S. Bakhtiari, B. Khaykovich, W. Cleary, "Pulsed Thermal Tomography Nondestructive Evaluation of Additively Manufactured Reactor Structural Materials," Transactions of the American Nuclear Society 121(1), 589-591 (2019).
11. A. Heifetz, D. Shribak, Z.L. Fisher, W. Cleary, "Detection of Defects in Additively Manufactured Metals Using Thermal Tomography," TMS 2021 150th Annual Meeting & Exhibition Supplemental Proceedings, 121-127 (2021).
12. E. D'Accardi, F. Palano, R. Tamborrino, D. Palumbo, A. Tatì, R. Terzi, U. Galietti. (2019). "Pulsed Phase Thermography Approach for the Characterization of Delaminations in CFRP and Comparison to Phased Array Ultrasonic Testing," Journal of Nondestructive Evaluation 38, 20 (2019).

13. C. Ibarra-Castanedo, A. Bendada and X. Maldague, “Thermographic Image Processing for NDT," IV Conferencia Panamericana de END, Buenos Aires (2007)
14. X. Zhang, J. Saniie, A. Heifetz, “Spatial Temporal Denoised Thermal Source Separation in Images of Compact Pulsed Thermography System for Qualification of Additively Manufactured Metals,” submitted to 2021 IEEE International Conference on Electro-Information Technology (EIT) (2021).
15. X. Zhang, T. Gonnot, J. Saniie, “Real-Time Face Detection and Recognition in Complex Background,” Journal of Signal and Information Processing 8, 99-112 (2017)
16. A. Gorry, "General Least-Squares Smoothing and Dfferentiation by the Convolution (Savitzky–Golay) Method,” Analytical Chemistry 62(6), 570-573 (1990).
17. A. Hyvärinen, “The Fixed-Point Algorithm and Maximum Likelihood Estimation for Independent Component Analysis,” Neural Processing Letters 10, 1-5 (1999).

Nuclear Science and Engineering (NSE) Division
Argonne National Laboratory
9700 South Cass Avenue, Bldg. 208
Argonne, IL 60439

www.anl.gov